the plant journal

SEB Society for Experimental Biology

The Plant Journal (2015) **82,** 547–555 doi: 10.1111/tpj.12824

The glucosinolate breakdown product indole-3-carbinol acts as an auxin antagonist in roots of *Arabidopsis thaliana*

Ella Katz[1], Sophia Nisani[1], Brijesh S. Yadav[1], Melkamu G. Woldemariam[2], Ben Shai[3], Uri Obolski[1], Marcelo Ehrlich[3], Eilon Shani[1], Georg Jander[2] and Daniel A. Chamovitz[1,*]

[1]*Molecular Biology and Ecology of Plants, Tel Aviv University, Ramat Aviv 69978, Israel,*

[2]*Boyce Thompson Institute, Ithaca, NY 14853, USA, and*

[3]*Cell Research and Immunology, Tel Aviv University, Ramat Aviv 69978, Israel*

Received 10 October 2014; revised 26 February 2015; accepted 4 March 2015; published online11 March 2015.
*For correspondence (e-mail dannyc@tauex.tau.ac.il).

SUMMARY

The glucosinolate breakdown product indole-3-carbinol functions in cruciferous vegetables as a protective agent against foraging insects. While the toxic and deterrent effects of glucosinolate breakdown on herbivores and pathogens have been studied extensively, the secondary responses that are induced in the plant by indole-3-carbinol remain relatively uninvestigated. Here we examined the hypothesis that indole-3-carbinol plays a role in influencing plant growth and development by manipulating auxin signaling. We show that indole-3-carbinol rapidly and reversibly inhibits root elongation in a dose-dependent manner, and that this inhibition is accompanied by a loss of auxin activity in the root meristem. A direct interaction between indole-3-carbinol and the auxin perception machinery was suggested, as application of indole-3-carbinol rescues auxin-induced root phenotypes. *In vitro* and yeast-based protein interaction studies showed that indole-3-carbinol perturbs the auxin-dependent interaction of Transport Inhibitor Response (TIR1) with auxin/3-indoleacetic acid (Aux/IAAs) proteins, further supporting the possibility that indole-3-carbinol acts as an auxin antagonist. The results indicate that chemicals whose production is induced by herbivory, such as indole-3-carbinol, function not only to repel herbivores, but also as signaling molecules that directly compete with auxin to fine tune plant growth and development.

Keywords: indole-3-carbinol, auxin, herbivory, *Arabidopsis thaliana*, glucosinolate.

INTRODUCTION

The phytochemical indole-3-carbinol (I3C) functions in cruciferous vegetables as a protective agent against foraging insects (Kim and Jander, 2007), and is used in humans as a dietary supplement with anti-carcinogenic properties (Aggarwal and Ichikawa, 2005). I3C is a breakdown product of glucosinolates, which are a diverse group of small molecules produced in the Cruciferae family, including *Brassica* vegetables, such as broccoli and cauliflower, and also *Arabidopsis thaliana* (Fahey *et al.*, 2001). Tissue damage from herbivores or physical means initiates hydrolysis of glucosinolates by endogenous plant β-thioglucosidases (commonly called myrosinases). Further catalysis and spontaneous degradation result in the formation of a wide variety of chemicals, including I3C (McDanell *et al.*, 1988; Halkier and Gershenzon, 2006). These glucosinolate breakdown products, in addition to their bioactive properties, cause the characteristic sharp taste of cruciferous vegetables (Bones and Rossiter, 1996; Keck and Finley, 2004; Kim and Milner, 2005). I3C is formed from the breakdown of indole-3-ymethylglucosinolate (I3M-GS), one of the most widely distributed glucosinolates (Agerbirk *et al.*, 2009). I3C, in turn, reacts with itself and a variety of other plant metabolites to form conjugates. In addition to their toxic effects on herbivorous insects, glucosinolate breakdown products may also signal further plant defense responses (Clay *et al.*, 2009); therefore, it is possible that I3M-GS breakdown triggers downstream responses in Arabidopsis and other crucifers. While specific roles for these I3C conjugates are slowly being revealed, most have as yet unknown functions in plant metabolism (Kim *et al.*, 2008).

Glucosinolate breakdown products have also been implicated in human health, with I3C in particular being studied as a therapeutic dietary supplement for women recovering from breast cancer (Bradlow, 2008). In human cells, I3C has been implicated in the inhibition of cell-cycle progression, induction of apoptosis, and inhibition of tumor invasion and metastasis (Meng *et al.*, 2000a,b; Firestone and Bjeldanes, 2003; Sarkar and Li, 2004; Fan *et al.*, 2006). The

© 2015 The Authors
The Plant Journal © 2015 John Wiley & Sons Ltd

mechanism by which I3C mediates these processes is unclear, although direct involvement with a variety of signaling pathways has been suggested (Li *et al.*, 2003).

While the toxic and deterrent effects of glucosinolate breakdown on herbivores and pathogens have been studied extensively, the secondary responses that are induced by I3C in plants remain relatively uninvestigated. Here we use the Arabidopsis root as a model system to elucidate pathways influenced by I3C. We show that I3C inhibits root elongation and competes with auxin perception *in vitro* and *in vivo*, suggesting that I3C acts as an auxin antagonist that has the potential to inhibit growth under biotic stress conditions.

RESULTS

Exogenous I3C is taken up by Arabidopsis seedlings

To confirm that I3C is taken up by Arabidopsis, seedlings were exposed for 2 h to medium containing 500 μM I3C, and analyzed by HPLC. The I3C-treated seedlings contained approximately 10 nmol g^{-1} I3C, whereas untreated controls had no detectable I3C (Figure 1). Similar accumulation of I3C was observed in *cyp79B2 cyp79B3* seedlings, which do not form indole glucosinolates (Hull *et al.*, 2000), and *tgg1 tgg2* seedlings, which do not degrade indole glucosinolates to I3C (Barth and Jander, 2006), an indication that the observed I3C accumulation is not the product of endogenous glucosinolate degradation.

Exogenous I3C treatment inhibits root elongation

To examine the effect of exogenous I3C on the growth of Arabidopsis roots, we first analyzed primary root lengths of Arabidopsis seedlings germinated on increasing concentrations of I3C. I3C inhibited root elongation in a dose-dependent manner (Figure 2a). Extrapolation of growth rates revealed 50% inhibition of root growth (IC_{50}) at 125 μM I3C, with 95% inhibition (IC_{95}) at approximately 400 μM (Figure 2b). Given that Arabidopsis seedlings contain 1.4 μg I3M-GS per gram root dry weight (Petersen *et al.*, 2002), corresponding to approximately 140 μM concentration, and the majority of this is converted to I3C after tissue damage, the local concentrations of I3C may be within the range of the IC_{50} for exogenous I3C.

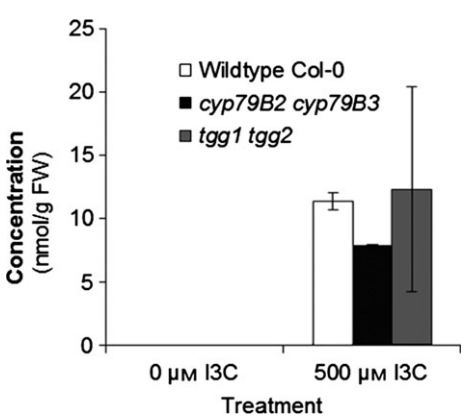

Figure 1. Uptake of I3C by Arabidopsis seedlings. Two-week-old Arabidopsis seedlings germinated in liquid MS medium were exposed to 500 μM I3C for 2 h or left untreated. I3C was not detected in untreated seedlings. Values are means ± SE of three replicates, each comprising 50 seedlings. The I3C levels in seedlings treated with I3C were higher than the levels in control seedlings for all three genotypes ($P < 0.05$, ANOVA followed by Tukey's HSD test). FW, fresh weight.

To study the kinetics of root growth inhibition after application of I3C, we grew seedlings on MS medium for 4 days, transferred them to solid medium with or without 400 μM I3C, and used time-lapse photography to monitor root elongation over 24 h (Movie S1). A decrease in the root elongation rate was immediately evident upon transfer to I3C medium. As shown in Figure 2(c), 60 min after transfer, the rate of root elongation of seedlings transferred to medium containing I3C was significantly lower than the rate of root elongation of seedlings transferred to medium without I3C (Student's *t* test, $P < 0.01$).

To determine whether this growth arrest is reversible, seedlings that had been germinated and grown on I3C for 8 days were transferred to fresh MS plates. Whereas the root elongation rate on 400 μM I3C was negligible compared with the rate on MS, the roots began to elongate upon transfer to MS medium at a rate approaching that of seedlings that had never been exposed to I3C (Figure S1). This indicates that the effect of I3C on root growth is reversible.

Other indole glucosinolate breakdown products influence root elongation

After tissue damage, I3M-GS breakdown proceeds in two directions, leading either to the formation of I3C and its derivates, or indole-3-acetonitrile (IAN) (Figure S2a) (Agerbirk *et al.*, 2009). We thus examined the effect of additional indole glucosinolate breakdown products (3, 3′-diindolylmethane, indole-3-carboxaldehyde and methyl-indole-3-carboxalate) on the growth of Arabidopsis roots. All chemicals tested inhibited root elongation (Figure S2b), thus we continued our analysis using I3C and IAN to represent the two breakdown pathways.

Exogenous I3C treatment inhibits auxin signaling

Inhibition of root growth is a typical phenotype of plants exposed to exogenous auxin, or plants with reduced endogenous auxin (List, 1969; Overvoorde *et al.*, 2010). Given the similar structures of I3C, IAN and 3-indoleacetic acid (IAA), with the difference being that I3C has a terminal hydroxyl group and IAN has a terminal cyanide, whereas IAA has a terminal carboxylic acid, we tested the hypothesis that in addition to IAA, I3C and IAN also induce auxin signaling in the root apical meristem. For this purpose, we used seedlings expressing *DR5::N7-VENUS*. In these

© 2015 The Authors

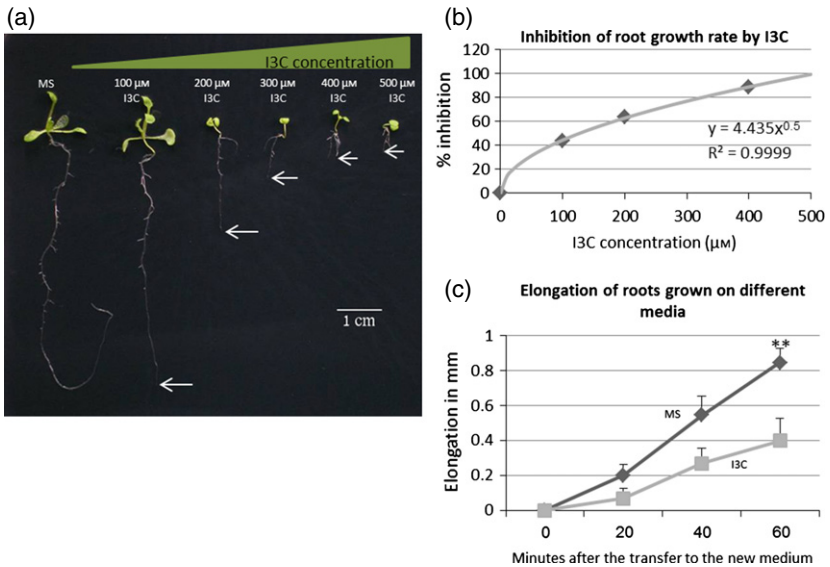

Figure 2. I3C treatment inhibits root elongation.
(a) Phenotypes of 14-day-old plants grown on increasing concentrations of I3C.
(b) Percentage inhibition of root elongation of seedlings grown on various concentrations of I3C. Inhibition was extrapolated based on regression fitting.
(c) Kinetics of root elongation inhibition by I3C. Seedlings were grown on MS medium for 4 days, and transferred to medium with or without 400 μM I3C. Root lengths for seven seedlings were measured every 20 min for each treatment. Asterisks indicate a statistically significant difference compared with I3C-containing medium (**$P < 0.01$, Student's *t* test). Values are means ± standard errors.

plants, the VENUS marker is a reporter for auxin responses (Ulmasov *et al.*, 1997; Heisler *et al.*, 2005). Seedlings were grown on MS medium for 6 days, treated with or without 200 μM I3C or 90 μM IAN for 6 h, and the YFP fluorescence was monitored. While IAN indeed increased the activity of the auxin reporter in epidermal and cortex cells, exogenous treatment with I3C reduced the activity of the reporter gene, contrary to our hypothesis (Figure 3a).

To determine whether the effect of I3C on the DR5::N7-VENUS signal is a direct response to changes in auxin perception and to elucidate its dynamics, we used plants expressing the VENUS protein fused to auxin interaction domain II of Aux/IAA (DII-VENUS) (Brunoud *et al.*, 2012). In these plants, the VENUS signal is sensitive to exogenous and endogenous auxin in a dose-dependent manner, without disrupting the activity of the auxin response machinery (Vernoux *et al.*, 2011; Brunoud *et al.*, 2012). Five-day-old DII-VENUS plants were treated with IAA, or both IAA and I3C, and the YFP fluorescence was monitored after 30 min using confocal microscopy. Thirty minutes following IAA treatment, low fluorescence of YFP was measured in the seedlings, indicating a high auxin signal. When the seedlings were treated with both IAA and I3C, an increase in YFP fluorescence was measured, suggesting that I3C inhibited IAA perception within 30 min (Figure 3b).

To determine whether the effect of I3C on auxin signaling is reversible, we measured the activity of the DR5::GUS reporter gene in seedlings that had been germinated on 400 μM I3C and were transferred to fresh MS plates after 4 days. As shown in Figure 3(c), seedlings grown on medium containing I3C show a low level of GUS activity at the root apical meristem, but 1 day after transfer to fresh medium without I3C, the GUS activity at the root apical meristem was high, indicating that the effect of exogenous I3C on auxin distribution is reversible.

I3C acts as an auxin antagonist

As I3C treatment led to a rapid reduction in auxin activity in the root apical meristem, and as the structure of I3C and auxin are very similar (Figure 4a), we hypothesized that I3C may act as an auxin antagonist. We further hypothesized that I3C interacts specifically with the auxin binding site of the Transport Inhibitor Response (TIR1) receptor (Gray *et al.*, 2001; Dharmasiri *et al.*, 2005), thus perturbing the interaction of TIR1/Auxin signaling F-Box (AFBs) with auxin/3-indoleacetic acid (Aux/IAAs) (Ken-ichiro Hayashi *et al.*, 2012).

To evaluate whether I3C is an auxin antagonist, we first modeled the potential interaction of I3C with TIR1, based on the crystal structure of auxin binding with TIR1 (Tan *et al.*, 2007). Our model predicts that while both I3C and IAN are able to associate with the auxin receptor site of TIR1, this putative interaction is with different regions of TIR1 (Figure 4b). Like IAA, I3C interacts with TIR1 chain B, while IAN putatively interacts with chain C (Figure 4b). Other I3C derivates also potentially interact with chain B (Figure S3). While I3C and IAN both inhibit root elongation, only I3C appears to negatively affect auxin signaling, potentially by competing with IAA with respect to binding to TIR1. As I3C and auxin differ in the residue attached to the 3rd carbon of their indole ring, I3C interaction with the auxin binding site of TIR1 may potentially perturb the docking of the Aux/IAA proteins, and thus directly inhibit the auxin response.

To test the hypothesis that I3C is an auxin antagonist, we analyzed the effect of I3C on three typical auxin responses: inhibition of root elongation, initiation of root hair formation, and promotion of lateral root formation. We monitored the root lengths of seedlings grown for 6 days on medium containing various concentrations of

© 2015 The Authors

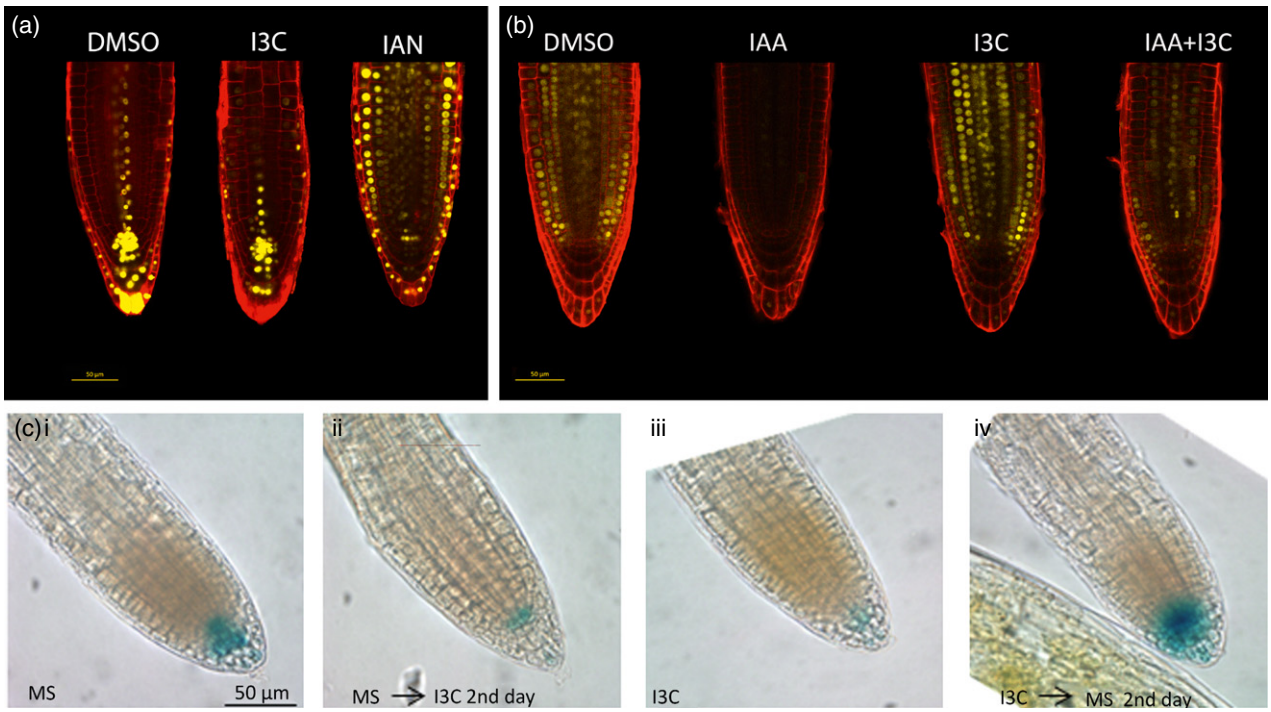

Figure 3. I3C reversibly inhibits auxin signaling in the root tip.
(a) Seedlings expressing *DR5::N7-VENUS* were grown on MS medium for 6 days, treated with 200 µM I3C or 90 µM IAN for 6 h, and imaged using confocal microscopy. Cell walls were stained using propidium iodide. Quantification of the relative integrated density of the VENUS fluorescence showed a significant decrease in the VENUS signal after I3C treatment (55% of the signal for the control plants), and a significant increase in the VENUS signal after IAN treatment (323% of the signal for the control plants). For each treatment, 5–10 seedlings were used ($P < 0.001$; Student's *t* test). Bar is 50 µm.
(b) I3C affects auxin signaling within 30 min. Five-day-old DII-VENUS seedlings grown on MS medium were treated for 30 min with 0.05 µM IAA, 300 µM I3C, or both, and imaged using confocal microscopy. Cell walls were stained using propidium iodide. Quantification of the relative integrated density of the VENUS fluorescence showed a significant decrease in the VENUS signal after IAA treatment (21% of the signal for the control plants), and a significant increase (173%) in the VENUS signal after treatment with both IAA and I3C compared to IAA-treated plants, suggesting that I3C inhibited the effect of IAA on auxin signaling within 30 min. For each treatment, 4–7 seedlings were used ($P < 0.01$; Student's *t* test). Bar is 50 µm.
(c) The effect of I3C on auxin signaling is reversible. DR5::GUS seedlings were grown on MS medium or on medium containing 400 µM I3C for 4 days, then transferred to the other medium for 2 days, the roots were photographed on the second day following transfer.

auxin, I3C, or both. As expected, roots of plants grown in the presence of auxin or I3C were significantly shorter than roots of plants grown on MS (Figure 5a). However, seedlings grown in the presence of both I3C and auxin exhibited roots that were significantly longer than those grown solely on auxin (but shorter than those grown on MS), suggesting that I3C partially antagonizes the effect of excess auxin. Similar results were obtained when assessing the number of root hairs and lateral roots on seedlings grown for 4 days on medium containing various concentrations of auxin, I3C, or both. As expected, the number of both root hairs and lateral roots was higher in plants treated with IAA (Figure 5b,c). Exposure to I3C led to a reduction in the number of root hairs and lateral roots. The roots of seedlings grown in the presence of both I3C and auxin exhibited a reduction in the number of root hairs and lateral roots compared to those grown on IAA alone, further indicating that I3C partially antagonizes the effect of excess auxin.

If I3C acts as an auxin antagonist, it is expected to directly manipulate the auxin perception machinery. Villalobos *et al.* (2012) previously showed that auxin promotes interaction between the auxin receptors TIR1/AFBs and Aux/IAA (IAA) family proteins in yeast two-hybrid assays. We utilized this system and found that I3C perturbs the interaction between TIR1 and IAA7 that is facilitated by auxin, but IAN does not (Figure 6a). Yeast expressing TIR1–LexA and Gal4–IAA7 fusion proteins were grown on medium containing auxin, I3C or IAN, or both I3C and auxin, or IAN and auxin. Expression of the β-galactosidase reporter was monitored 4 days after spotting. As a negative control, we used LexA yeast expressing TIR1 and an empty plasmid instead of IAA7, and as a positive control, we used LexA yeast expressing Pto and AvrPto, which are known to interact (Bogdanove and Martin, 2000). As shown in Figure 6(a), the interaction between TIR1 and IAA7 was facilitated when the yeast grew on medium containing auxin, consistent with previous studies (Villalobos *et al.*, 2012). This interaction was diminished when we added I3C to the growth medium in addition to auxin, but not when IAN was added to the auxin. The reduction in interaction was apparent at 50 µM I3C, and almost complete at 150 µM

© 2015 The Authors

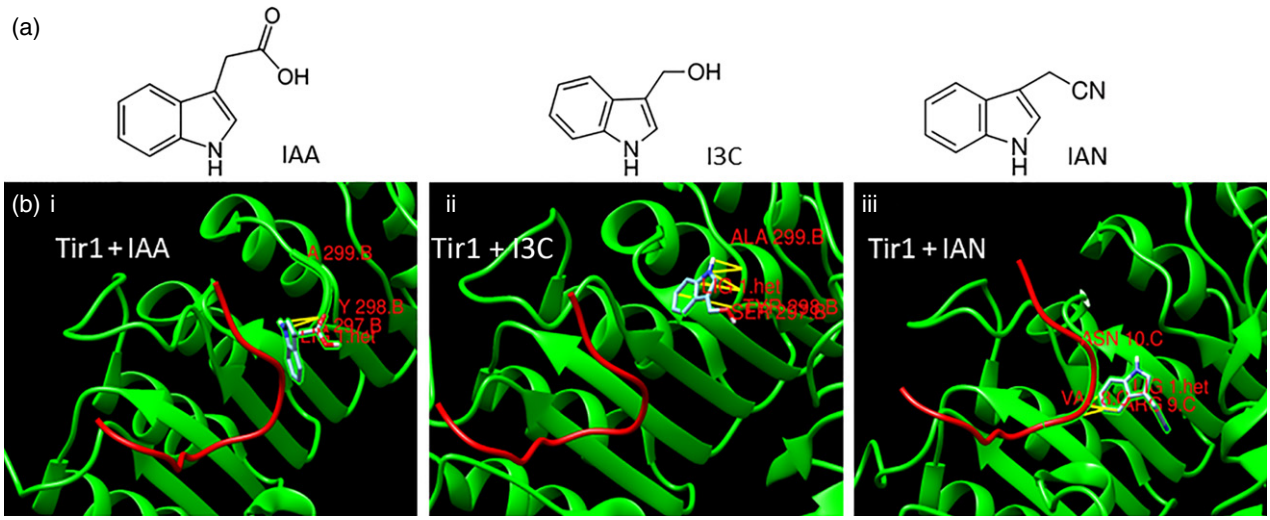

Figure 4. Modeling of I3C/IAN binding to TIR1.
(a) Structure of auxin (IAA), I3C and IAN.
(b) Predicted interaction of I3C (i) or IAN (iii) with TIR1 based on auxin binding (i). Blue represents I3C (ii), IAN (iii) or IAA (i), and yellow lines represent hydrogen bonds between TIR1 and IAA/I3C/IAN. IAA and I3C bind to chain B of TIR1 (green helix) with binding energies of −4.5 kcal mol^{-1} for TIR1/IAA and −4.1 kcal mol^{-1} for TIR1/I3C. IAN binds to chain C of TIR1 (red chain), with a binding energy of −4.5 kcal mol^{-1}.

Figure 5. I3C rescues IAA-driven root phenotypes.
(a) Seedlings were grown on MS medium containing 0.2 μM IAA, 300 μM I3C, or both. At 6 days, seedlings were photographed (a′) and root length was measured.
(b) Seedlings were grown on MS medium for 4 days, and then transferred to medium containing 0.2 μM IAA, 300 μM I3C, or both. At 8 days, seedlings were photographed (b′) and the number of root hairs was counted.
(c) Seedlings were grown on MS medium for 4 days, and then transferred to medium containing 0.5 μM IAA, 200 μM I3C, or both. At 8 days, seedlings were photographed (c′) and the number of lateral roots was counted. Multiple comparisons between treatments using ANOVA followed by a Tukey's HSD test revealed that all treatments were statistically significantly different ($P < 0.01$), except for IAA+I3C in comparison with I3C, for all measures. Values are means ± standard errors. For each treatment, 7–45 seedlings were used.

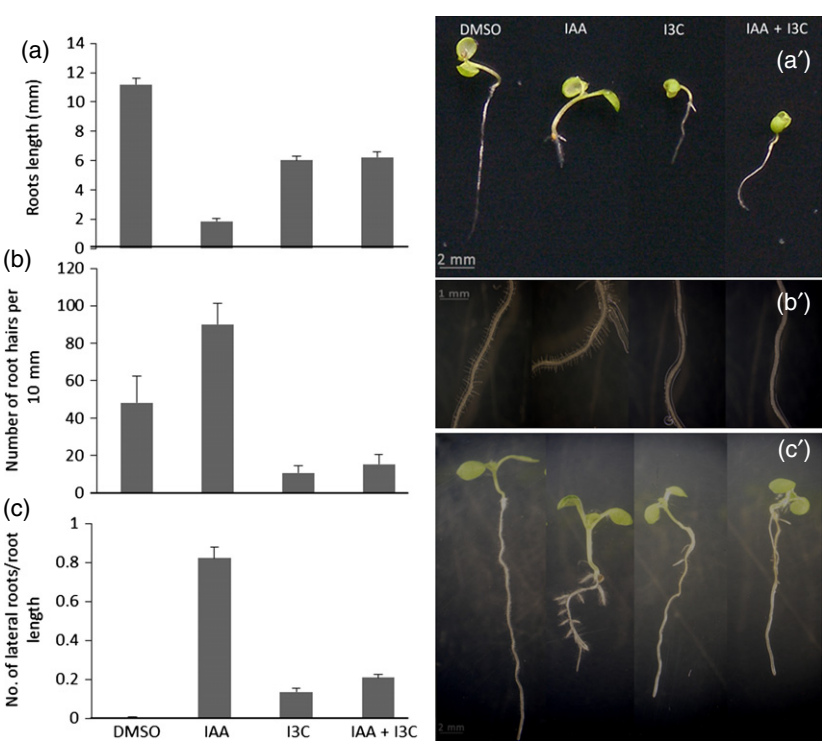

I3C. While a slight reduction in yeast growth was noticed in the presence of I3C, this did not inhibit the interaction of Pto and AvrPto (positive control).

To further confirm the yeast two-hybrid assay results, we performed an *in vitro* pull-down assay using *in vitro* translated TIR1–Myc and recombinant GST–IAA3 protein purified from *Escherichia coli* (Parry *et al.*, 2009). The proteins were pulled down using GST beads in the presence or absence of 100 μM IAA or 100 μM IAA plus 10 mM I3C, separated by SDS–PAGE, and the interaction between TIR1 and IAA3 was detected using an anti-c-Myc antibody. As expected, the *in vitro* interaction between TIR1 and IAA3 was apparent only when auxin was present in the reaction mixture (Figure 6b, lane III) as indicated by the high TIR1/IAA3 ratio.

© 2015 The Authors

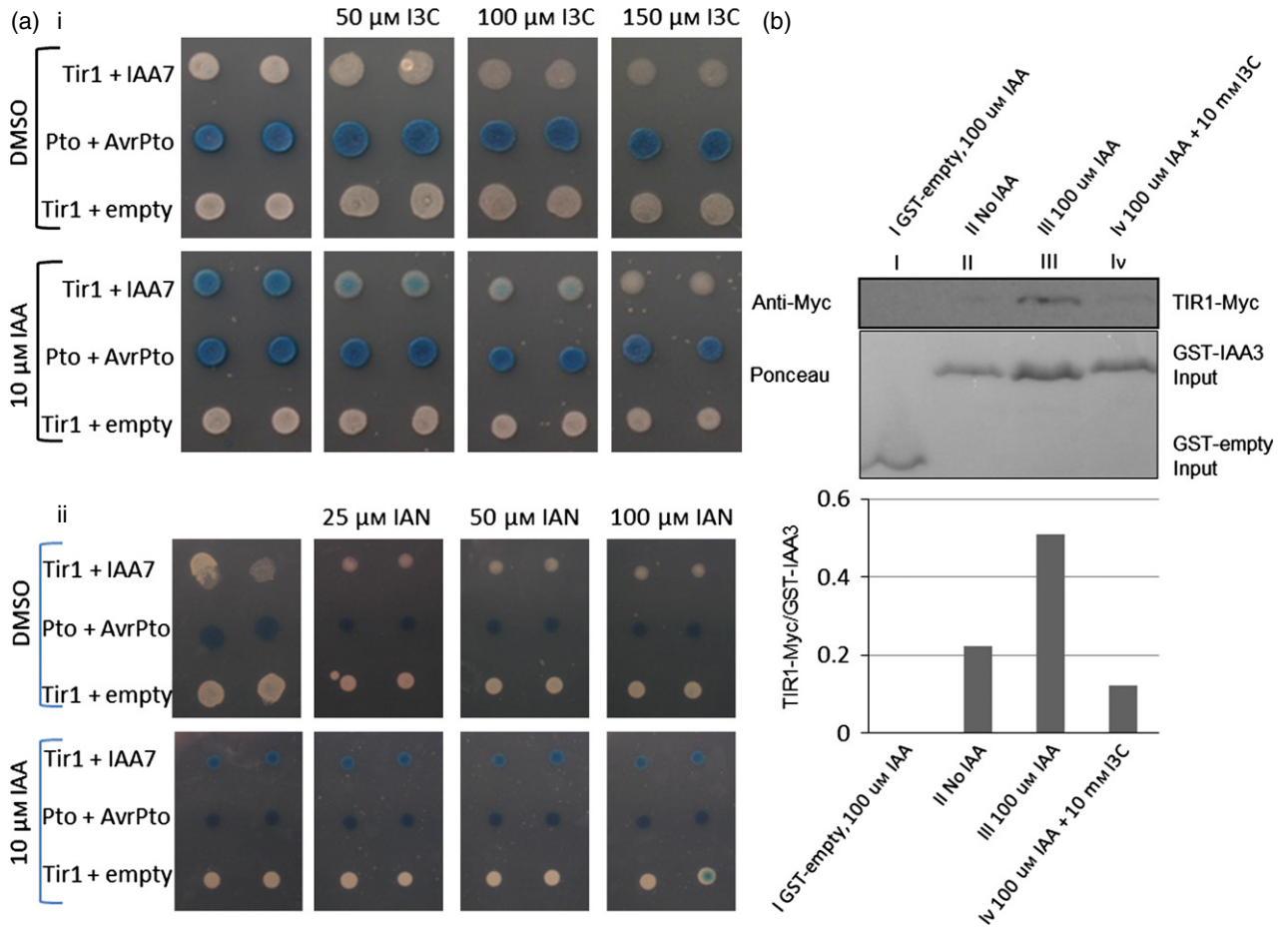

Figure 6. I3C perturbs auxin-dependent interaction of TIR1 and IAA proteins in yeast and *in vitro*.
(a) LexA yeast expressing TIR1 or Tir1 and IAA7 was grown on medium containing IAA, I3C or IAN, or both I3C and auxin (i), or IAN and auxin (ii). Expression of the β-galactosidase reporter expression was monitored 4 days after spotting.
(b) An *in vitro* pull-down assay of TIR1–Myc and GST–IAA3 was performed using recombinant GST–IAA3 and *in vitro* translated TIR1–Myc. The pull-down assays were incubated at 4°C for 1 h in the presence (lanes I and III) or absence (lane II) of 100 µM auxin, or in the presence of 10 mM I3C and 100 µM auxin (lane Iv).

Addition of I3C to the reaction mixture resulted in a reduction in the TIR1 and IAA3 ratio (Figure 6b, lane Iv), indicating that I3C inhibited the auxin-mediated interaction between TIR1 and IAA3. Taken together, the results of these experiments suggest that I3C modulates auxin action in an antagonistic manner.

DISCUSSION

Here we show that the glucosinolate breakdown product indole-3-carbinol (I3C) inhibits root elongation, probably acting as an auxin antagonist. We first observed that I3C inhibits roots growth in a dose-dependent manner, and that this effect is reversible. As inhibition of root elongation is a typical auxin exposure phenotype, we hypothesized that I3C affects auxin signaling in the root, and indeed found that I3C treatment rapidly and reversibly reduced auxin signaling in the root tip.

Our results indicate that I3C reduces auxin signaling by acting as an auxin antagonist on the TIR1 receptor. Several lines of evidence support this conclusion. First, molecular modeling predicted that I3C associates with the auxin binding site of the TIR1 auxin receptor. Second, at the molecular level, auxin reporter genes were down-regulated after I3C treatment. Third, at the physiological level, I3C partially rescued the effect of IAA on several root phenotypes. Fourth, at the level of protein–protein interactions, I3C directly perturbed the auxin-dependent interaction of TIR1 with IAA proteins both in yeast and *in vitro*.

This mode of action is apparently specific for I3C but not all I3M-GS breakdown products, as although IAN also inhibited root elongation, its influence on auxin signaling was different to that of I3C. Thus I3M-GS breakdown products probably influence plant development at multiple levels.

Taken together, the results presented here clearly demonstrate that I3C influences plant growth by directly modulating auxin signaling. The implication is that chemicals whose production is induced by herbivory, such as I3C, function not only to repel the herbivore, but also as signal-

© 2015 The Authors

ing molecules within the plant. Thus, our results suggest that I3C is a defensive phytohormone that modulates auxin signaling, leading to growth arrest.

Salicylic acid and jasmonic acid, the two best-studied plant defense signaling molecules, are likely to have originally functioned as small molecule metabolites that provided direct defense against herbivores and pathogens (Jander and Clay, 2011). Jasmonic acid not only induces numerous plant defense responses, but also influences primary metabolism, for instance reducing the synthesis of sugars and amino acids (Adio *et al.*, 2011). Our results suggest that other plant defensive metabolites may also have secondary functions in regulating aspects of plant metabolism, providing diversity in defense-related plant signaling pathways. Such diversity of defensive metabolites in defense-related plant signaling pathways is beneficial for the plant, as herbivores and pathogens are less likely to be able to mount effective counter-measures.

The idea that herbivory also affects plant development is not new. Many studies have shown that herbivory induces plant growth arrest (Adler and Wink, 2001; Poveda *et al.*, 2003). Such arrest has most often been attributed to changes in resource allocation, e.g. the growth differentiation balance hypothesis (Gershenzon, 1994; Massad *et al.*, 2012). We propose that the growth arrest may also be signaled directly by the induced chemicals, i.e. I3C in this case. Thus glucosinolate breakdown to I3C after herbivory has two outcomes, i.e. I3C repels the herbivore, while at the same time inducing growth arrest within the plant.

Although our studies used exogenously applied I3C, the concentrations are within the amounts of indole glucosinolates found endogenously in Arabidopsis seedlings (approximately 140 μM). Furthermore, as not all of the exogenous I3C is taken up by the plant (Figure 1), the I3C concentration within the plant after treatment is lower than the exogenous concentrations used. Thus, given that we observed approximately 40% root growth inhibition at 100 μM I3C, this concentration is potentially physiologically relevant and similar to what would be perceived locally by a plant that has an insect chewing on its roots. Accordingly, the relative concentrations of auxin and I3C in the cell may well be within the range of those used here. Auxin gradients form within the root tip to drive growth and development. While it is not clear what the exact levels of auxin concentration are in different cell types and at the subcellular level, studies have estimated that the IAA activity in roots is within the physiological range (nanomolar to micromolar) (Petersson *et al.*, 2009; Band and King, 2012; Bargmann *et al.*, 2013), and is probably low following wounding (Cheong *et al.*, 2002). Hence, the concentration of IAA after wounding may be approximately 100 times lower than the concentration of I3C after wounding.

Finally, a recent study showed that volatile indoles released from soil bacteria modulate auxin signaling in roots (Bailly *et al.*, 2014). Thus, the idea that indole-containing metabolites negatively influence auxin signaling appears to be an emerging paradigm.

EXPERIMENTAL PROCEDURES

Plant materials and growth assays

The Arabidopsis strains used in this work were all in the Columbia-0 (Col-0) background. The transgenic and mutant lines have been described previously: DR5::GUS (Ulmasov *et al.*, 1997), DR5::N7-VENUS (Heisler *et al.*, 2005), DII-VENUS (Brunoud *et al.*, 2012), *cyp79B2 cyp79B3* (Hull *et al.*, 2000), and *tgg1 tgg2* (Barth and Jander, 2006). Seeds were cultivated in Petri plates using medium containing 0.8% agar, half-strength Murashige and Skoog salts (MS), and 1% sucrose, pH 5.7. The Petri plates were placed in chambers at 22°C under light/dark conditions of 16 h white light at 75 μmol m^2 sec^{-1} and 8 h darkness, at 55% relative humidity. For root phenotype experiments, plates were placed vertically in the chambers.

Preparation of indole metabolites

Indole-3-carbinol (I3C), 3-indoleacetic acid (IAA/auxin), indole-3-acetonitrile (IAN), 3,3′-diindolylmethane, indole-3-carboxaldehyde and methyl-indole-3-carboxalate (Sigma, https://www.sigmaaldrich.com/) were dissolved in dimethylsulfoxide to produce 1 M solutions, and stored in the dark at −20°C.

4D imaging system

Seedlings were grown for 4 days on MS medium. The seedlings were transferred to MS medium with or without 400 μM I3C and photographed every 20 min over 24 h using a 4D imaging system developed at the laboratory of Hillel Fromm (Department of Molecular Biology and Ecology of Plants, Tel Aviv University, Israel). Root length was measured using IMAGEJ software (http://imagej.nih.gov/ij/).

GUS reporter assay

DR5::GUS seedlings were grown on agar plates with or without I3C, and stained using X-Gluc as described by Weigel and Glazebrook (2002). The roots were transferred to slides with drops of double-distilled water, and photographed using a Zeiss Axioplan2 microscope (www.zeiss.com) and CELL A software, (Olympus, www.olympus-global.com).

Confocal microscopy

Four- to six-day-old seedlings from marker strains were transferred to liquid MS containing 200 μM I3C or dimethylsulfoxide. After treatment, seedlings were submerged in 0.005 mg ml^{-1} propidium iodide in double-distilled water, placed on microscope slides, and imaged using a Zeiss LSM780 confocal microscope with ×20/NA 0.8. The fluorescence emission was collected between 590 and 720 nm (band pass) for propidium iodide, and between 520 and 580 nm (band pass) for yellow fluorescent protein (YFP). YFP fluorescence was quantified using IMAGEJ software (http://imagej.nih.gov/ij/).

Measurement of I3C levels by HPLC

I3C was dissolved in 80% methanol to prepare a 1 μg ml^{-1} stock solution. A serial dilution was used to generate a standard curve for subsequent quantification of I3C in plant samples. Samples were separated using a Waters 2790 pump system coupled to a

© 2015 The Authors

Waters 2996 photodiode array detector (Waters, http://www.waters.com/). We used a Kinetex column (Phenomenex, www.phenomenex.com/; 5 μm, 18C, 100 Å, 150 × 4.60 mm) and a solvent system comprising water (solvent A) and acetonitrile (solvent B, 90% v/v in water). The HPLC running conditions were: 0–5 min, 100% A; 5–24 min, 90% A; 24–29 min, 30% A; 29–35 min, 0% A; 35–40 min, 90% A, with a flow rate of 1 ml min^{-1}.

Quantification of I3C uptake by seedlings

Seeds of wild-type Col-0, *tgg1 tgg2* and *cyp79B2 cyp79B3* were surface-sterilized using 30% sodium hypochlorite containing 0.05% v/v Tween-20, followed by rinsing in 70% ethanol and five rinses with sterile water (Weigel and Glazebrook, 2002). Seeds were planted in liquid MS medium, and grown for 2 weeks under a 16 h light/8 h dark regime at 22°C. Half of the 2-week-old seedlings were treated with 500 μM I3C, and the rest were left as untreated controls. After 2 h, the seedlings were rinsed three times with deionized water, collected in liquid nitrogen, weighed, and lyophilized to dryness. The dried samples were ground to a fine powder, homogenized in 0.8 ml of 80% methanol, and heated for 15 min at 75°C. After centrifugation for 5 min at 15 000 ***g***, the supernatant was loaded onto a 250 μl Sephadex A25 column (Pharmacia Fine Chemicals, www.pfizer.com/). Samples were eluted using 2 × 250 μl of 80% methanol and 2 × 200 μl water, the eluents were combined and dried under vacuum, and the residue was re-dissolved in 100 μl of 80% methanol. After filtering by centrifugation through Multi-Screen-HV filter plates (Millipore, www.emdmillipore.com/), 20 μl of the solution was analyzed by HPLC as described above.

Molecular modeling of I3C docking to TIR1

AutoDock Vina (Trott and Olson, 2010) was used for molecular docking analysis of I3C with the TIR1 protein from *A. thaliana* (PDB ID 2P1Q). The two-dimensional structure of the I3C substrate, taken from the National Center for Biotechnology Information PubChem server (www.ncbi.nlm.nih.gov/), was converted into 3D coordinates via the CORINA server (www.molecular-networks.com/online_demos/corina_demo). The Lamarckian genetic algorithm in AutoDock was used to perform the automated molecular dockings. Docking of I3C with TIR1 protein was performed in two steps. In the preliminary step, dockings were performed to identify the potential binding sites on the TIR1 protein, and in the second step, the whole surface of the protein was covered with large grid maps, created by AutoGrid. The *x*, *y* and *z* grid dimensions were set to 72 Å, with grid points separated by 0.375 Å.

Yeast two-hybrid assays

Yeast two-hybrid assays were performed as described previously (Prigge *et al.*, 2010). The *TIR1* bait vector pGILDA and the *IAA7* prey vector pB42AD (Prigge *et al.*, 2010) were co-transformed into *Saccharomyces cerevisiae* strain EGY48 as described previously (Gietz and Schiestl, 2007). The negative control comprised yeast expressing pGILDA containing *TIR1* and an empty pB42AD vector. As a positive control, we used yeast expressing the Pto and AvrPto proteins (Bogdanove and Martin, 2000).

In vitro pull down assays

In vitro pull-down assays were performed as described by Parry *et al.* (2009). Briefly, a TIR1–Myc fusion protein was synthesized using the TNT T7 coupled wheatgerm extract system (Promega, www.promega.com/). GST–IAA3 protein was expressed in the *E. coli* BL21 DE3 strain and purified using glutathione agarose beads (Sigma) in lysis buffer (50 mM Tris, 100 mM NaCl, 10% glycerol, 0.1% Tween-20, pH 7, and protease inhibitors, Roche, www.roche.com/). Then 25 μl of extract were incubated with GST–IAA3 beads in 200 μl lysis buffer (pH 5.7) in the presence or absence of 100 μM IAA or 100 μM IAA plus 10 mM I3C, at 4°C for 1 h. Unbound proteins were washed twice for four min, at 4°C on microchromatography columns (Bio-Rad, www.bio-rad.com/) using the same buffer. Proteins were eluted using elution buffer comprising 100 mM Tris and 15 mg ml^{-1} reduced glutathione (Sigma), pH 8, separated by SDS–PAGE and detected using monoclonal anti-c-Myc (Provided by Eran Bacharach, Department of Cell research and Immunology, Tel Aviv University, Israel). To standardize the input, the membranes were stained using 0.1% Ponceau-S in 5% acetic acid solution, band intensities were quantified using IMAGEJ software (http://imagej.nih.gov/ij/), and the ratio between the TIR1 and IAA3 input bands was calculated.

ACKNOWLEDGEMENTS

This research was supported by a grant from the Binational Agricultural Research and Development Fund (IS-4505-12R) to D.A.C. and G.J. B.Y. was supported by a fellowship from the PBC (Planning and Budgeting Committee) Fellowship Program for Outstanding Post-Doctoral Researchers from India. We thank Mark Estelle (Section of Cell and Developmental Biology, University of California, San Diego) for the TIR1 and Aux/IAA constructs. We thank Manely Rabanim, Hila Behar, Mor Sela, Ora Hazak, Tal Sherman, Roye Nuriel, Guido Sessa (Department of Molecular Biology and Ecology of Plants, Tel Aviv University, Israel) and Efrat Elis (Department of Cell Research and Immunology, Tel Aviv University, Israel) for technical assistance or providing reagents.

SUPPORTING INFORMATION

Additional Supporting Information may be found in the online version of this article.

Figure S1. The effect of I3C on root inhibition is reversible.

Figure S2. I3M-GS breakdown products inhibit root elongation.

Figure S3. Modeling of binding of I3C derivatives to TIR1.

Movie S1. Kinetics of inhibition of root elongation by I3C.

REFERENCES

Adio, A.M., Casteel, C.L., De Vos, M., Kim, J.H., Joshi, V., Li, B., Juery, C., Daron, J., Kliebenstein, D.J. and Jander, G. (2011) Biosynthesis and defensive function of *N*-delta-acetylornithine, a jasmonate-induced Arabidopsis metabolite. *Plant Cell*, **23**, 3303–3318.

Adler, L.S. and Wink, M. (2001) Transfer of quinolizidine alkaloids from hosts to hemiparasites in two *Castilleja-Lupinus* associations: analysis of floral and vegetative tissues. *Biochem. Syst. Ecol.* **29**, 551–561.

Agerbirk, N., De Vos, M., Kim, J.H. and Jander, G. (2009) Indole glucosinolate breakdown and its biological effects. *Phytochem. Rev.* **8**, 101–120.

Aggarwal, B.B. and Ichikawa, H. (2005) Molecular targets and anticancer potential of indole-3-carbinol and its derivatives. *Cell Cycle*, **4**, 1201–1215.

Bailly, A., Groenhagen, U., Schulz, S., Geisler, M., Eberl, L. and Weisskopf, L. (2014) The interkingdom volatile signal indole promotes root development by interfering with auxin signalling. *Plant J.* **80**, 758–771.

Band, L.R. and King, J.R. (2012) Multiscale modelling of auxin transport in the plant-root elongation zone. *J. Math. Biol.* **65**, 743–785.

Bargmann, B.O., Vanneste, S., Krouk, G. *et al.* (2013) A map of cell type-specific auxin responses. *Mol. Syst. Biol.* **9**, 688.

Barth, C. and Jander, G. (2006) Arabidopsis myrosinases TGG1 and TGG2 have redundant function in glucosinolate breakdown and insect defense. *Plant J.* **46**, 549–562.

Bogdanove, A.J. and Martin, G.B. (2000) AvrPto-dependent Pto-interacting proteins and AvrPto-interacting proteins in tomato. *Proc. Natl Acad. Sci. USA*, **97**, 8836–8840.

© 2015 The Authors

Bones, A.M. and Rossiter, J.T. (1996) The myrosinase-glucosinolate system, its organisation and biochemistry. *Physiol. Plant.* **97**, 194–208.

Bradlow, H.L. (2008) Review. Indole-3–carbinol as a chemoprotective agent in breast and prostate cancer. *In Vivo*, **22**, 441–445.

Brunoud, G., Wells, D.M., Oliva, M. *et al.* (2012) A novel sensor to map auxin response and distribution at high spatio-temporal resolution. *Nature*, **482**, 103–106.

Cheong, Y.H., Chang, H.S., Gupta, R., Wang, X., Zhu, T. and Luan, S. (2002) Transcriptional profiling reveals novel interactions between wounding, pathogen, abiotic stress, and hormonal responses in Arabidopsis. *Plant Physiol.* **129**, 661–677.

Clay, N.K., Adio, A.M., Denoux, C., Jander, G. and Ausubel, F.M. (2009) Glucosinolate metabolites required for Arabidopsis innate immune response. *Science*, **323**, 95–101.

Dharmasiri, N., Dharmasiri, S. and Estelle, M. (2005) The F-box protein TIR1 is an auxin receptor. *Nature*, **435**, 441–445.

Fahey, J.W., Zalcmann, A.T. and Talalay, P. (2001) The chemical diversity and distribution of glucosinolates and isothiocyanates among plants. *Phytochemistry*, **56**, 5–51.

Fan, S., Meng, Q., Auborn, K., Carter, T. and Rosen, E.M. (2006) BRCA1 and BRCA2 as molecular targets for phytochemicals indole-3–carbinol and genistein in breast and prostate cancer cells. *Br. J. Cancer*, **94**, 407–426.

Firestone, G.L. and Bjeldanes, L.F. (2003) Indole-3–carbinol and 3-3′-diindolylmethane antiproliferative signaling pathways control cell-cycle gene transcription in human breast cancer cells by regulating promoter-Sp1 transcription factor interactions. *J. Nutr.* **133**, 2448S–2455S.

Gershenzon, J. (1994) Metabolic costs of terpenoid accumulation in higher plants. *J. Chem. Ecol.* **20**, 1281–1328.

Gietz, R.D. and Schiestl, R.H. (2007) Large-scale high-efficiency yeast transformation using the LiAc/SS carrier DNA/PEG method. *Nat. Protoc.* **2**, 38–41.

Gray, W.M., Kepinski, S., Rouse, D., Leyser, O. and Estelle, M. (2001) Auxin regulates SCF(TIR1)-dependent degradation of AUX/IAA proteins. *Nature*, **414**, 271–276.

Halkier, B.A. and Gershenzon, J. (2006) Biology and biochemistry of glucosinolates. *Annu. Rev. Plant Biol.* **57**, 303–333.

Heisler, M.G., Ohno, C., Das, P., Sieber, P., Reddy, G.V., Long, J.A. and Meyerowitz, E.M. (2005) Patterns of auxin transport and gene expression during primordium development revealed by live imaging of the Arabidopsis inflorescence meristem. *Curr. Biol.* **15**, 1899–1911.

Hull, A.K., Vij, R. and Celenza, J.L. (2000) Arabidopsis cytochrome P450s that catalyze the first step of tryptophan-dependent indole-3-acetic acid biosynthesis. *Proc. Natl Acad. Sci. USA*, **97**, 2379–2384.

Jander, G. and Clay, N. (2011) New synthesis–plant defense signaling: new opportunities for studying chemical diversity. *J. Chem. Ecol.* **37**, 429.

Keck, A.S. and Finley, J.W. (2004) Cruciferous vegetables: cancer protective mechanisms of glucosinolate hydrolysis products and selenium. *Integr. Cancer Ther.* **3**, 5–12.

Ken-ichiro Hayashi, J.N., Hirose, M., Kuboki, A., Shimada, Y., Kepinski, S. and Nozaki, H. (2012) Rational design of an auxin antagonist of the SCF-TIR1 auxin receptor complex. *ACS Chem. Biol.* **7**, 590–598.

Kim, J.H. and Jander, G. (2007) *Myzus persicae* (green peach aphid) feeding on Arabidopsis induces the formation of a deterrent indole glucosinolate. *Plant J.* **49**, 1008–1019.

Kim, Y.S. and Milner, J.A. (2005) Targets for indole-3–carbinol in cancer prevention. *J. Nutr. Biochem.* **16**, 65–73.

Kim, J.H., Lee, B.W., Schroeder, F.C. and Jander, G. (2008) Identification of indole glucosinolate breakdown products with antifeedant effects on *Myzus persicae* (green peach aphid). *Plant J.* **54**, 1015–1026.

Li, Y., Li, X. and Sarkar, F.H. (2003) Gene expression profiles of I3C- and DIM-treated PC3 human prostate cancer cells determined by cDNA microarray analysis. *J. Nutr.* **133**, 1011–1019.

List, A. Jr (1969) Transient growth responses of the primary roots of *Zea mays*. *Planta*, **87**, 1–19.

Massad, T.J., Dyer, L.A. and Vega, C.G. (2012) Costs of defense and a test of the carbon-nutrient balance and growth-differentiation balance hypotheses for two co-occurring classes of plant defense. *PLoS One*, **7**, e47554.

McDanell, R., McLean, A.E., Hanley, A.B., Heaney, R.K. and Fenwick, G.R. (1988) Chemical and biological properties of indole glucosinolates (glucobrassicins): a review. *Food Chem. Toxicol.* **26**, 59–70.

Meng, Q., Goldberg, I.D., Rosen, E.M. and Fan, S. (2000a) Inhibitory effects of indole-3–carbinol on invasion and migration in human breast cancer cells. *Breast Cancer Res. Treat.* **63**, 147–152.

Meng, Q., Qi, M., Chen, D.Z., Yuan, R., Goldberg, I.D., Rosen, E.M., Auborn, K. and Fan, S. (2000b) Suppression of breast cancer invasion and migration by indole-3–carbinol: associated with up-regulation of BRCA1 and E-cadherin/catenin complexes. *J. Mol. Med.* **78**, 155–165.

Overvoorde, P., Fukaki, H. and Beeckman, T. (2010) Auxin control of root development. *Cold Spring Harb. Perspect. Biol.* **2**, a001537.

Parry, G., Calderon-Villalobos, L.I., Prigge, M., Peret, B., Dharmasiri, S., Itoh, H., Lechner, E., Gray, W.M., Bennett, M. and Estelle, M. (2009) Complex regulation of the TIR1/AFB family of auxin receptors. *Proc. Natl Acad. Sci. USA*, **106**, 22540–22545.

Petersen, B.L., Chen, S., Hansen, C.H., Olsen, C.E. and Halkier, B.A. (2002) Composition and content of glucosinolates in developing *Arabidopsis thaliana*. *Planta*, **214**, 562–571.

Petersson, S.V., Johansson, A.I., Kowalczyk, M., Makoveychuk, A., Wang, J.Y., Moritz, T., Grebe, M., Benfey, P.N., Sandberg, G. and Ljung, K. (2009) An auxin gradient and maximum in the Arabidopsis root apex shown by high-resolution cell-specific analysis of IAA distribution and synthesis. *Plant Cell*, **21**, 1659–1668.

Poveda, K., Steffan-Dewenter, I., Scheu, S. and Tscharntke, T. (2003) Effects of below- and above-ground herbivores on plant growth, flower visitation and seed set. *Oecologia*, **135**, 601–605.

Prigge, M.J., Lavy, M., Ashton, N.W. and Estelle, M. (2010) *Physcomitrella patens* auxin-resistant mutants affect conserved elements of an auxin-signaling pathway. *Curr. Biol.* **20**, 1907–1912.

Sarkar, F.H. and Li, Y. (2004) Indole-3–carbinol and prostate cancer. *J. Nutr.* **134**, 3493S–3498S.

Tan, X., Calderon-Villalobos, L.I., Sharon, M., Zheng, C., Robinson, C.V., Estelle, M. and Zheng, N. (2007) Mechanism of auxin perception by the TIR1 ubiquitin ligase. *Nature*, **446**, 640–645.

Trott, O. and Olson, A.J. (2010) AutoDock Vina: improving the speed and accuracy of docking with a new scoring function, efficient optimization, and multithreading. *J. Comput. Chem.* **31**, 455–461.

Ulmasov, T., Murfett, J., Hagen, G. and Guilfoyle, T.J. (1997) Aux/IAA proteins repress expression of reporter genes containing natural and highly active synthetic auxin response elements. *Plant Cell*, **9**, 1963–1971.

Vernoux, T., Brunoud, G., Farcot, E. *et al.* (2011) The auxin signalling network translates dynamic input into robust patterning at the shoot apex. *Mol. Syst. Biol.* **7**, 508.

Villalobos, C., Caballero, E., Sanz-Blasco, S. and Nunez, L. (2012) Study of neurotoxic intracellular calcium signalling triggered by amyloids. *Methods Mol. Biol.* **849**, 289–302.

Weigel, D. and Glazebrook, J. (2002) *Arabidopsis: A Laboratory Manual*. Cold Sping Harbor, NY: Cold Spring Harbor Laboratory Press.

© 2015 The Authors
The Plant Journal © 2015 John Wiley & Sons Ltd,